Simulation of an Inert Membrane Reactor for the Synthesis of Maleic Anhydride

M. Pedernera, R. Mallada, M. Menéndez, and J. Santamaría
Dept. of Chemical and Environmental Engineering, Faculty of Science, University of Zaragoza, 50009 Zaragoza, Spain

A simulation of an inert membrane reactor in the partial oxidation of butane to maleic anhydride in high butane concentrations (2–13%) is presented. A porous membrane was used to distribute oxygen to a fixed bed of VPO catalyst, to which butane was fed. Two different reactor configurations were simulated: a standard inert membrane reactor, in which oxygen permeates inward from the shell side and the catalyst is packed on the tube side; an outward flow inert membrane reactor, in which the catalyst bed is packed on the shell side and oxygen flows outward from the tube side. The model explains the different performances of both types of reactor in terms of the interaction between the oxygen and hydrocarbon concentration profiles and the temperature profiles that are obtained with both reactor configurations.

Introduction

Research in the field of inorganic membranes in general and membrane reactors in particular continues to expand rapidly, as evidenced by several reviews that have appeared during 1999 (Saracco et al., 1999; Dixon, 1999; Coronas and Santamaría, 1999a,b; Tavolaro and Drioli, 1999). While most works dealing with separations use dense (such as Pd-based membranes, solid electrolytes) or microporous (microporous silica, zeolites) membranes in order to obtain a high separation selectivity, mesoporous membranes have been intensely used in reaction applications, where permselectivity is often less important than attaining adequate flux or maintaining tight control on the mode of contact between reactants. Applications of mesoporous membranes in reactors (see, for instance, Dixon, 1999; Coronas and Santamaría, 1999a) include the use of (1) *catalytic membranes* to attain control of the mode of contact (segregated feeds) and to enhance reactant conversion (flowthrough membranes, membranes in gas–liquid reactions), and (2) *inert membranes* for equilibrium shift and reactant distribution. This work is concerned with the last type of application, where a porous membrane is used to distribute one of the reactants to a fixed bed of catalyst. The membrane is not catalytically active, and thus this type of reactor is frequently known as an inert membrane reactor (IMR).

Most of the activity in the area of IMRs based on mesoporous membranes has been devoted to the preparation and characterization of the membranes and their application to reaction, while a smaller number of works addressed the simulation of reacting systems. The main differences among the modeling works published to date concern the reactor configuration, the complexity of the simulation (one- or two-dimensional models, co- or countercurrent, etc.), and the treatment of permeation through the membrane. Sun and coworkers (1990) did some early work using a one-dimensional model and Knudsen flow to simulate the use of IMRs for equilibrium shift in dehydrogenation reactions and in general in processes where the number of moles changed with conversion. Tsotsis et al. (1992) also employed a one-dimensional model to simulate a more complex reactor configuration: a double packed-bed reactor separated by a catalytic membrane in hydrogen-producing reactions; in this case, the transport of H_2 across the membrane was taken into account by means of Fick's law. The same approach was used in a two-dimensional model to simulate alkane dehydrogenation in an IMR by Bindjouli et al. (1994), who used orthogonal collocation in the numerical solution. All of these works considered the use of membranes for equilibrium displacement.

Correspondence concerning this article should be addressed to J. Santamaría.
M. Pedernera is on leave of absence from the Universidad Nacional del Sur, Bahia Blanca, Argentina.

The reactant distribution application also has been modeled with a similar degree of complexity. With a few exceptions [e.g., the work of Tsai et al. (1995), who simulated the use of a dense perovskite membrane as oxygen distributor in syngas production from methane], the bulk of the work published in this area concerns the use of porous membranes, where permselectivity is not required. Cheng et al. (1995) simulated methane oxidative coupling with a simple one-dimensional model in which a membrane produced a uniform distribution of oxygen to a fixed-bed reactor, and Tonkovich et al. (1996) used a similar approach for methane oxidative coupling and also for the oxidative dehydrogenation of ethane. Coronas and coworkers (1997) simulated methane oxidative coupling with a one-dimensional model, and for the first time incorporated the influence of the unwanted catalytic activity of the membrane on the reaction. Yang et al. (1998) used a two-dimensional isothermal model to simulate the partial oxidation of methane to formaldehyde, in which oxygen transport across the membrane was governed by either Knudsen diffusion or Fick's law. Finally, Tellez et al. (1999) employed a one-dimensional nonisothermal model for the oxidative dehydrogenation of butane, in which oxygen transport across the membrane was described by an extended Fick's law.

The preceding works showed that a simplified treatment of permeation is often sufficient to obtain a good description of the behavior of IMRs in reactant-distribution applications. However, when the molar fluxes of different species and concentration profiles within the membrane are to be predicted (such as, for instance, when modeling catalytic membrane reactors: Saracco et al., 1995; Harold and Lee, 1997), a more sophisticated approach is needed, and the so-called dusty gas model (DGM) becomes the tool of choice for simulation of permeation. Similarly, when the calculation of radial concentration and/or temperature profiles is required to explain the behavior of an IMR, a two-dimensional approach is needed.

In an earlier work, Mallada et al. (2000a) experimentally tested two different IMR configurations for the partial oxidation of butane to maleic anhydride (MA) over VPO catalysts, under butane concentrations considerably higher than those generally used in industry. One of the reactors (termed IMR) distributed oxygen inwardly, permeating from the shell side to a bed of catalyst packed on the inner side of a tubular membrane. In the other reactor, termed the outward flow inert membrane reactor (OFIMR), the catalyst bed was packed on the shell side, and oxygen permeated outward from the tube side (see Figure 1). Other than that, the reactors were essentially the same, except for the fact that the catalyst load in the OFIMR was higher; however, their performance was markedly different, with a clear advantage for the OFIMR in terms of the selectivity (and MA yield) at the same conversion level. A qualitative explanation was postulated involving a different evolution of the concentration and temperature profiles in both reactors, which could give rise to the observed differences. However, no direct measurement of these profiles was possible, and the speculations were not supported by a reactor model.

In this work we have carried out the simulation of the oxidation of butane to MA in both types of membrane reactor (IMR and OFIMR). To our knowledge, this is the first time that a two-dimensional model has been used to simulate a membrane reactor in reactant-distribution applications (that is, where the inert membrane is used to supply the reactant to a fixed bed of catalyst). The results of the simulation agree well with the experimental findings of the previous work (Mallada et al., 2000a), and allow us to explain the different performances of both types of membrane reactor.

Experimental Studies

Some experiments have been carried out in order to test the capability of the model employed to predict the results

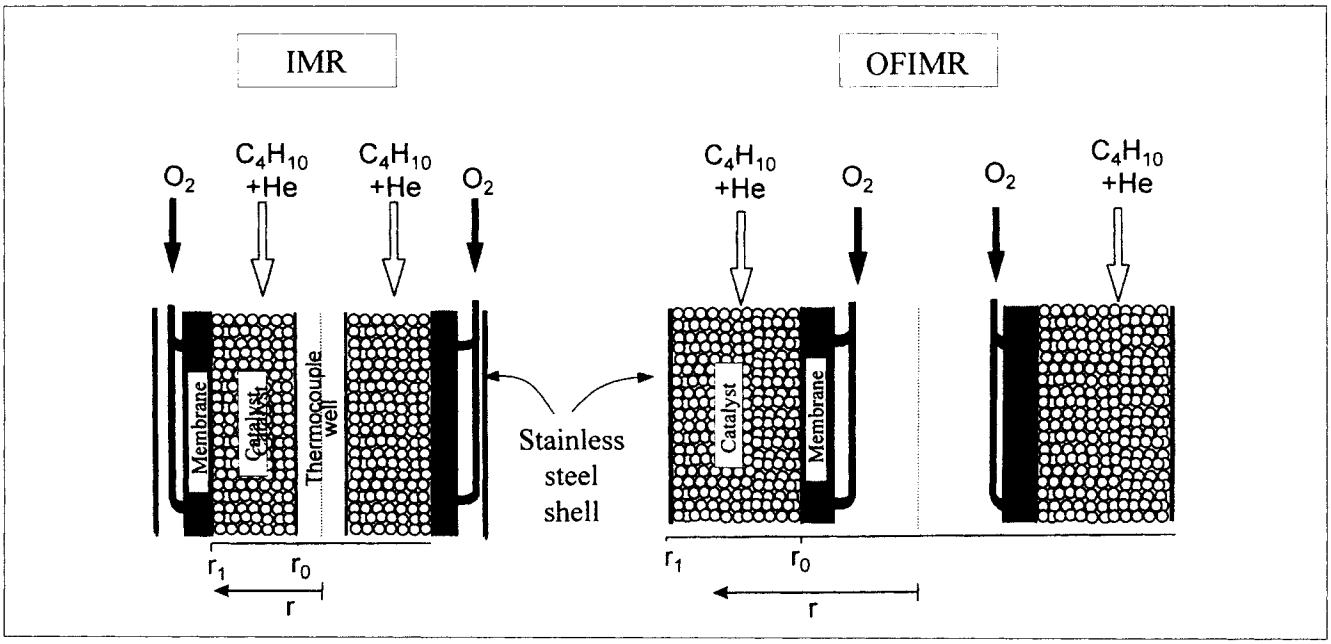

Figure 1. Two types of membrane reactor used.

obtained in both membrane reactors. A description of the reaction system is given elsewhere (Mallada et al., 2000a), and a scheme of the flow arrangement in both reactors is presented in Figure 1. Briefly, the VPO catalyst used was supplied, already in an active form, by DuPont, within the framework of the European project BRPR-CT95-0046. It was sieved to a particle size of 160–320 microns and loaded (2.5–3.5 g in the IMR; 16–18 g in the OFIMR) as a packed bed of annular cross section (between a quartz thermowell and the membrane in the IMR; between the membrane and the outer steel shell in the OFIMR), according to the scheme in Figure 1. Mass flow-controlled streams of butane, oxygen, and He were fed to the appropriate side of the membrane, as shown in Figure 1, and the products were analyzed by an on-line gas chromatograph. All the results presented were collected at steady state, after a stabilization period.

In addition to the experiments carried out with the membrane reactor, a separate experimental program was undertaken to determine the kinetics of the reaction. These experiments were carried out in a quartz microreactor and with W/F values sufficiently small to work (for butane) under differential conditions (conversion was less than 5%). Several alternative kinetic schemes were considered, among them a dual-site Mars–van Krevelen mechanism that assumed two different types of sites on the catalyst: selective sites, giving maleic anhydride, and nonselective sites, giving CO and CO_2. After model discrimination this kinetic scheme was chosen as the best fitting model on the basis of the differential reactor results. Further, with these kinetics it was possible to predict the behavior observed in a fixed-bed reactor under integral conditions without further parameter fitting. The results of the kinetic study will be published elsewhere (Mallada et al., 2000b). The rates of reaction in the model selected are given by the following expressions:

$$r_{MA} = \frac{k_1 P_B P_{O_2}^{0.5}}{\left[1 + k_4 \frac{P_B}{P_{O_2}^{0.5}} + k_5 P_{O_2}^{0.5}\right]} \quad (1)$$

$$r_{CO} = \frac{k_2 P_B}{\left[1 + k_4 \frac{P_B}{P_{O_2}^{0.5}} + k_5 P_{O_2}^{0.5}\right]} \quad (2)$$

$$r_{CO_2} = \frac{k_3 P_B}{\left[1 + k_4 \frac{P_B}{P_{O_2}^{0.5}} + k_5 P_{O_2}^{0.5}\right]} \quad (3)$$

where r_{MA}, r_{CO} and r_{CO_2} are the rates of formation of maleic anhydride, CO and CO_2, respectively, and k_1 to k_5 are the kinetic coefficients (Mallada et al., 2000b). Equations 1–3 were used directly in the simulation of the membrane reactors.

Model Development

A two-dimensional, steady-state model has been developed for the simulation of both IMR and OFIMR, with the dimensions given in Table 1. In the model, inter- and intraparticle mass- and heat-transfer resistances were assumed to be negligible. This is reasonable, because the particle size and gas velocities used in the membrane reactor experiments are within the range selected for kinetic studies. Also, it was assumed that the contribution of axial dispersion in the mass and heat balances could be neglected. This also seems reasonable in view of the reactor-length to particle-size ratio used and the range of Reynolds numbers involved.

Table 1. Parameter Values Used in the Simulation*

T_o (K)		673
L (m)		15×10^{-2}
r_1 (m)	OFIMR	8.75×10^{-3}
	IMR	3.35×10^{-3}
r_0 (m)	OFIMR	5×10^{-3}
	IMR	1.5×10^{-3}
D_{er} (m^2/s)		2×10^{-6}
δ (m)		0.00175
Avg. Cp (at 673 K) (kJ/kmol·K)		40.8
Avg. μ (at 673 K) (Pa·s)		1.1×10^{-5}
k_{er} (W/m·K)		0.27

*Kinetic parameters are given in Mallada et al. (2000b).

The steady-state mass balance for each of the species i present in the reactor takes into account the convective transport in the axial and radial directions, the diffusion in the radial direction, and the rate of disappearance/generation by chemical reaction:

$$G_z \frac{\partial y_i}{\partial z} = \frac{1}{r}\frac{\partial}{\partial r}\left(rD_{er}C\frac{\partial y_i}{\partial r}\right) - (-r_i)\rho_L - G_r\frac{\partial y_i}{\partial r}, \quad (4)$$

where G_z and G_r are the molar fluxes in the axial and radial directions, respectively. As can be deduced from Figure 1, G_r becomes null at $r = r_0$ (external radius of the quartz thermowell) in the IMR, and at $r = r_1$ (stainless-steel wall) in the OFIMR. For inner positions the variation of G_r can be obtained from the overall mass balance, assuming that, for any radial position, there is a constant rate of increase of G_z in the axial direction ($\partial G_z/\partial z$ = constant). The resulting expression for the OFIMR is

$$G_r = G_{r(r=r_0)}\frac{r_0}{\left(r_1^2 - r_0^2\right)}\left[\frac{r_1^2}{r} - r\right], \quad (5)$$

and for the IMR,

$$G_{r(r=r_1)}\frac{r_1}{\left(r_1^2 - r_0^2\right)}\left[r - \frac{r_0^2}{r}\right]. \quad (6)$$

The pressure of oxygen on the upstream side of the membrane was taken as constant, while the total pressure at the permeate (reaction) side was calculated using the Ergun equation and taking into account the variation of the total flow rate as permeation proceeds. When pure oxygen was permeated from the shell side, the rate of oxygen permeation was calculated from the dusty gas model (DGM) equations

Table 2. Membrane Characteristics

Membrane	Silica Loading (wt.%)	$K_0 \times 10^{10}$ (m)	$B_0 \times 10^{17}$ (m^2)
IMR	15	23.1	11.5
OFIMR	5.6	7.51	1.49

(Mason and Malinauskas, 1983) as

$$\frac{N_i}{\Delta P} = \frac{D^e_{i,k}}{RT\delta} + \frac{B_0}{RT\delta\mu} P_m \tag{7}$$

$$D^e_{ik} = K_0 \sqrt{\frac{8RT}{\pi M_i}}; \quad K_0 = \frac{2}{3} r_p \frac{\epsilon}{\tau}; \quad B_0 = \frac{1}{8} r_p^2 \frac{\epsilon}{\tau}, \tag{8}$$

where K_0 and B_0 are geometric parameters of the membrane that depend on the tortuosity (τ) and porosity (ϵ) of the material. Both K_0 and B_0 were experimentally obtained by measuring the permeation of single gases through the membrane and using Eq. 7 to fit the permeation fluxes obtained for different total pressures and pressure gradients between both sides of the membrane. The values obtained for K_0 and B_0 for different membranes used in this work are given in Table 2. These values depend strongly on the loading (wt. %) and distribution of the pore-filling material, which explain the widely different values obtained for different membranes.

The heat balance in both the IMR and the OFIMR is given by

$$\frac{\partial T}{\partial z} = \frac{1}{G_z \Sigma_i y_i Cp_i} \left(\frac{1}{r} \frac{\partial}{\partial r} \left(k_{er} r \frac{\partial T}{\partial r} \right) + \rho_L \sum_{j=1}^{m} r_j (-\Delta H_{r_j}) \right). \tag{9}$$

Boundary conditions

At the reactor entrance ($z = 0$) in both reactors,

$$y_i = y_{i0} \quad \text{and} \quad T = T_0 \quad \text{for} \quad r_0 \le r \le r_1. \tag{10}$$

The boundary conditions in the radial direction depend on the type of reactor used, due to the fact that oxygen enters the reactor at different positions (at $r = r_1$ in the IMR and at $r = r_0$ in the OFIMR, see Figure 1).

For the OFIMR at $r = r_0$ the convective term is equal to the diffusive term for all species except for oxygen, where the term corresponding to oxygen permeation appears. Also, at $r = r_0$ there is heat transfer to the incoming gas. We can then write

$$r = r_0 \begin{cases} G_r y_i - D_{er} C \dfrac{\partial y_i}{\partial r} = 0 & i \neq \mathrm{O}_2 \\ G_r y_{\mathrm{O}_2} - D_{er} C \dfrac{\partial y_{\mathrm{O}_2}}{\partial r} = N_{\mathrm{O}_2} \\ k_{er} \dfrac{\partial T}{\partial r} = U'(T - T_{\mathrm{O}}), \end{cases} \tag{11}$$

where N_{O_2} is calculated using the DGM, as explained earlier. On the other hand, the reactor shell is impervious for all species, and therefore only heat transfer takes place in the OFIMR at $r = r_1$

$$r = r_1 \begin{cases} \dfrac{\partial y_i}{\partial r} = 0 & i = 1, nc \\ k_{er} \dfrac{\partial T}{\partial r} = U(T - T_{cm}), \end{cases} \tag{12}$$

where T_{cm} is the temperature of the cooling medium (air) outside the reactor.

For the IMR, the corresponding boundary conditions are found by taking into account the different reactor schemes (Figure 1). Thus, at the quartz rod ($r = r_0$), there is no heat or mass transfer:

$$r = r_0 \begin{cases} \dfrac{\partial y_i}{\partial r} = 0 & i = 1, nc \\ \dfrac{\partial T}{\partial r} = 0; \end{cases} \tag{13}$$

at the membrane wall ($r = r_1$) the convection and diffusion terms are equivalent to those already shown for the OFIMR (Eq. 11), and the heat transfer term is also included:

$$r = r_1 \begin{cases} G_r y_i - D_{er} C \dfrac{\partial y_i}{\partial r} = \mathrm{O} & i \neq \mathrm{O}_2 \\ G_r y_{\mathrm{O}_2} - D_{er} C \dfrac{\partial y_{\mathrm{O}_2}}{\partial r} = N_{\mathrm{O}_2} \\ k_{er} \dfrac{\partial T}{\partial r} = U(T - T_{cm}). \end{cases} \tag{14}$$

The effective diffusivity (D_{er}) and the effective thermal conductivity (k_{er}) of the catalyst bed in the radial direction were calculated using the expressions given by Froment and Hoffman (1987), and by de Wasch and Froment (1972), respectively. It must be noticed that these correlations were developed for fixed-bed reactors and the validity of their use in the IMR and OFIMR (where a significant contribution of convective radial flow may be present) is questionable. However, since there are no correlations in the literature that are directly applicable for inert membrane reactors, we have employed the expressions just indicated; it seems reasonable to expect that any errors introduced will likely have a similar effect on the simulations of the IMR and OFIMR, and therefore should not affect the conclusions of this work.

Table 1 gives the parameter values used in the simulation. To solve the mathematical model, the radial coordinate was discretized using a finite differences scheme (23 radial internal points), leading to a set of ODEs, which were finally integrated by means of a Gear algorithm (Gear, 1971). Preliminary numerical experiments showed that a stable and sufficiently accurate solution (further increasing the number of intervals did not change the results) was obtained with $\Delta\zeta = 0.045$ (dimensionless radial coordinate) and $\Delta\phi = 0.005$ (dimensionless axial coordinate).

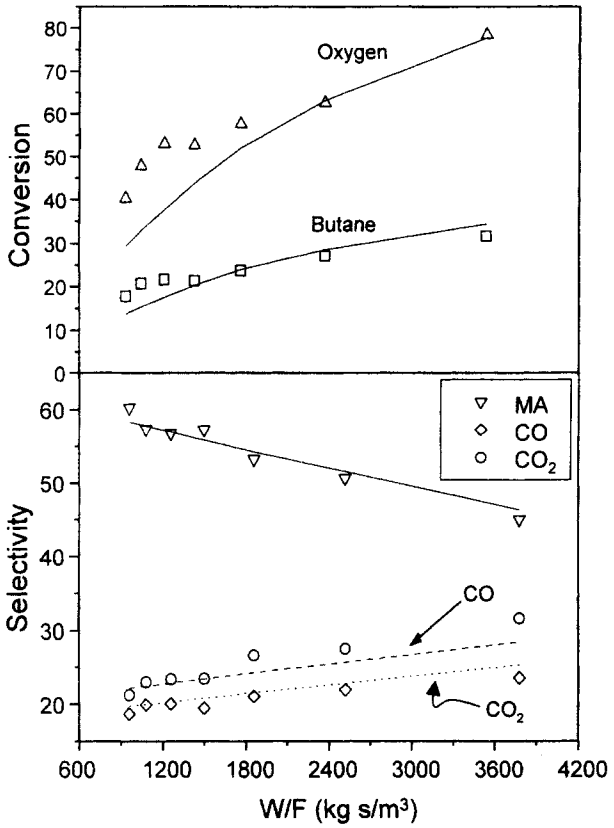

Figure 2. Experimental (symbols) vs. calculated (continuous lines) results.

Butane and oxygen conversions and selectivity to the different products as a function of the space time in the IMR. Overall feed ratio: $C_4H_{10}/O_2/He = 10/20/70$, $T_o = 400°C$.

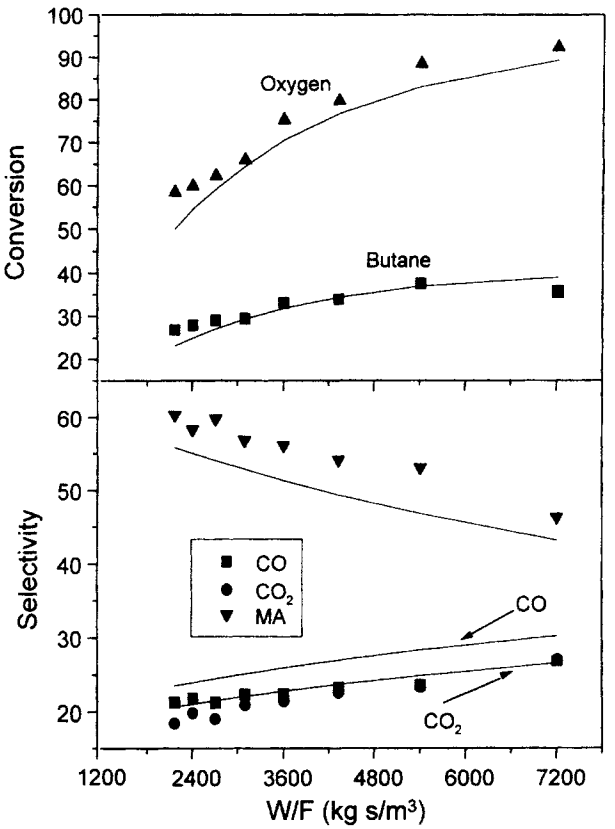

Figure 3. Experimental (symbols) vs. calculated (continuous lines) results.

Butane and oxygen conversions and selectivity to the different products as a function of the space time in the OFIMR. Overall feed ratio: $C_4H_{10}/O_2/He = 10/20/70$, $T_o = 400°C$.

Results and Discussion

Comparison with experimental results

Figures 2 and 3 show the model predictions (butane and oxygen conversions, selectivity to CO, CO_2, and MA) and the experimental data for the IMR and OFIMR, respectively. It can be seen that the trends are correctly predicted, although there are differences between the model predictions and some of the experimental data points. The largest deviations are in the calculation of oxygen conversion at low W/F values in the IMR (Figure 2) and of the selectivity to CO in the OFIMR (Figure 3). Other than that, the agreement can be considered as satisfactory, especially if one takes into account that the predictions of Figures 2 and 3 (membrane reactors, integral conversions) stem from kinetics obtained under differential conditions in a fixed-bed microreactor (at butane conversions lower than 5%), without further data fitting.

More importantly, the two-dimensional model presented here was able to adequately simulate the improvement of selectivity obtained with the OFIMR with respect to the IMR. Figure 4 shows the MA yields that were experimentally obtained in both reactors, along with the model predictions. The predictions obtained with a one-dimensional model (i.e., considering homogeneous temperature and composition along the radius at any axial position) are also shown. It might be noticed that the predictions of butane and oxygen conver-

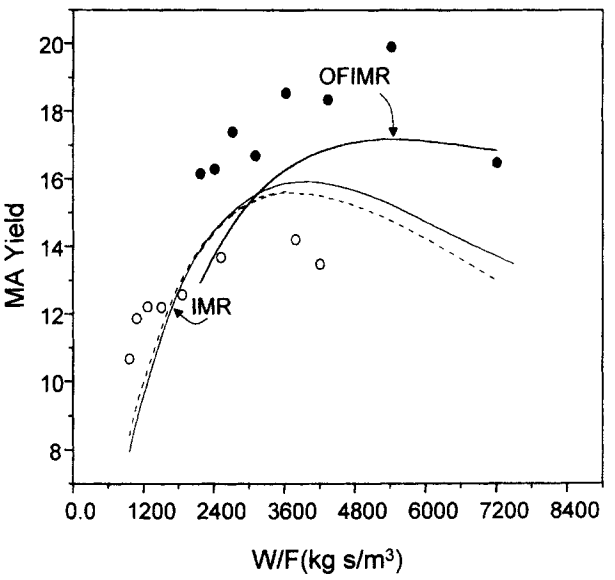

Figure 4. MA yield as a function of space time in IMR and OFIMR.

The symbols correspond to experimental data points. Conditions as in Figure 3. Continuous lines, predictions of the 2-D model; dotted line, predictions of the 1-D model, identical for both reactors.

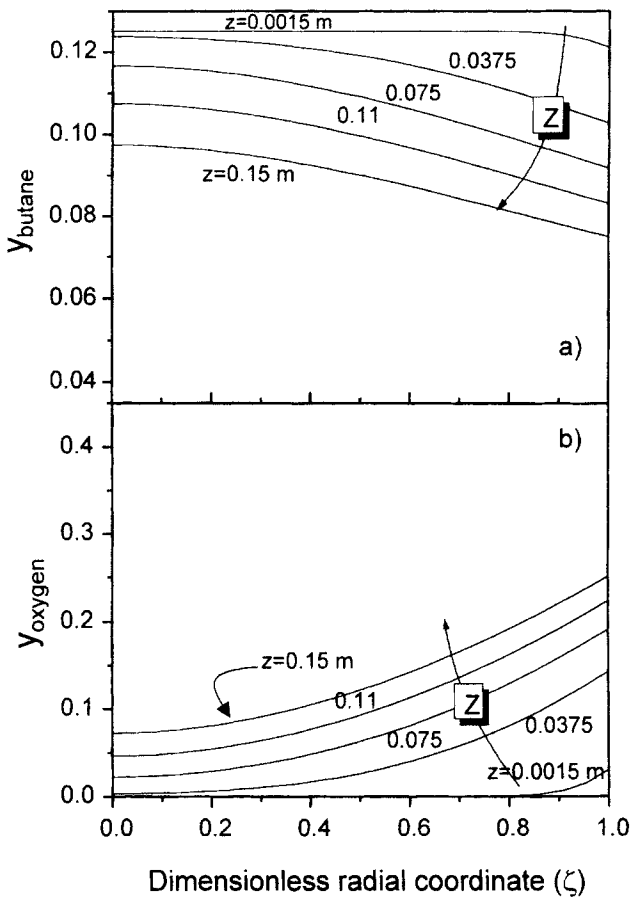

Figure 5. Radial concentrations of butane (a) and oxygen (b) for different axial positions in IMR.

W/F = 3,900 g·s/m^3 (STP). Other conditions as in Figure 3. $\zeta = 1$, membrane wall ($r = r_1$ in Figure 1); $\zeta = 0$, external wall of the quartz thermowell ($r = r_0$ in Figure 1).

sions obtained with the one-dimensional model (not shown) were satisfactory, with accuracy comparable to that of the two-dimensional model; however, the selectivity-conversion behavior predicted for the IMR and OFIMR was identical, that is, the explanation of the different performances of the two reactors requires consideration of radial temperature and composition profiles, which the one-dimensional model cannot take into account.

Simulation results: Comparison between the IMR and OFIMR

As just discussed, the two-dimensional model allows us to take the temperature and concentration profiles in both reactors into account. Figure 5 shows the butane and oxygen concentration profiles calculated for the IMR, for different values of z (axial coordinate). Close to the reactor entrance ($z = 0.0015$ m), oxygen is only starting to permeate in the IMR, and the reaction atmosphere contains mainly butane and He at any radial position. As we move further into the bed, the oxygen supply through the reactor wall continues and its concentration increases, while that of butane decreases. The highest oxygen/butane ratios are always reached near the membrane wall ($\zeta = 1$), and their values increase as we move toward the reactor exit ($z = 0.15$ m).

The VPO catalyst is sensitive to the reaction atmosphere, as demonstrated by Soejarto et al. (1996), who used alternately oxidizing and reducing conditions to provide evidence of the relatively fast and reversible transformation between the different VPO phases. Also, Rodemerck et al. (1997) investigated the behavior of VPO catalysts, with average degrees of oxidation ranging from 3.2 to 4.9. Catalysts with an average oxidation state of 3.7 behaved nonselectively, giving only butene, butadiene, furan, CO, and CO_2. This agrees with a number of studies (e.g., Centi et al., 1984; Hutchings et al., 1994; Ait-Lachgar et al., 1994) that have clearly established that a moderately high oxidation state is needed for MA synthesis, and that active and selective catalysts mainly contain V^{4+} with some V^{5+} centers.

In view of the concentration profiles presented in Figure 5, it can be concluded that the catalyst in contact with reducing atmospheres (i.e., where the hydrocarbon to oxygen ratio is high), will be located in the entrance region of the reactor ($z \to 0$). For higher values of z, the more reduced catalyst will be found near the reactor axis ($\zeta \to 0$). Under these circumstances ($z \to 0$ and/or $\zeta \to 0$), the catalyst surface will likely be reduced beyond the optimum oxidation state, with the corresponding decrease in selectivity. The situation in the OFIMR is rather different as shown in Figure 6. As in the IMR, the more highly reducing atmospheres (high butane-to-oxygen ratios) occur away from the porous wall (where oxygen permeation takes place and the oxygen concentration is highest), but the reducing region is now found at $\zeta = 1$, that is, at the outermost radial positions, near the reactor shell (which for the OFIMR corresponds to $r = r_1$ in Figure 1).

The model was used to calculate the evolution of the fraction of active selective (θ_{oo}) and nonselective (θ_o) sites along the reactor radius (as described in Mallada et al., 2000b). The ratio of selective to nonselective sites (θ_{oo}/θ_o), is directly related to the reaction selectivity. Its radial variation is plotted in Figure 7 for different axial positions in the reactor. It can be seen that the evolution of the θ_{oo}/θ_o ratio is determined by the reaction atmosphere: in the IMR the lowest values are found at $\zeta = 0$, where a highly reducing atmosphere exists, and the opposite is true for the OFIMR (lowest θ_{oo}/θ_o ratio at $\zeta = 1$). In both reactors the θ_{oo}/θ_o ratio increases toward the reactor exit, that is, as the oxygen concentration in the reactor increases. Although an increase of the oxygen concentration increases both θ_{oo} and θ_o, the concentration of the more selective (and more oxidized) θ_{oo} sites increase faster, and so θ_{oo}/θ_o increases. Comparison of Figures 7a and 7b also indicates that the increase of θ_{oo}/θ_o with radial position is much steeper in the OFIMR, and that it is in this reactor where the highest values of the θ_{oo}/θ_o ratio are found at any axial position.

Let us now consider the temperature profiles. Exothermic reactions take place (butane oxidation to MA, CO, and CO_2) in both the IMR and the OFIMR, and heat losses occur at $\zeta = 1$ (outer wall, see Figure 1). Therefore, the radial temperature profiles present maxima at $\zeta = 0$ in both reactors, as shown in Figure 8, although the temperature drop is greater in the OFIMR, with a larger diameter. The temperature drop in the OFIMR reaches a value close to 4°C at $z = 0.0375$ m.

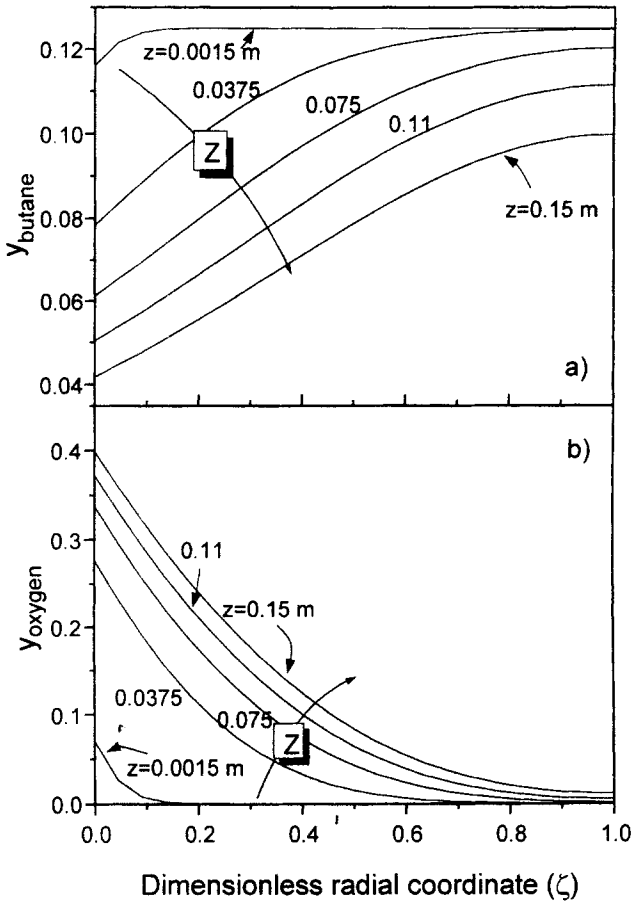

Figure 6. Radial concentration profiles of butane (a) and oxygen (b) for different axial positions in OFIMR.

$\zeta = 0$, membrane wall ($r = r_0$ in Figure 1); $\zeta = 1$, stainless-steel shell ($r = r_1$ in Figure 1). Same conditions as in Figure 5.

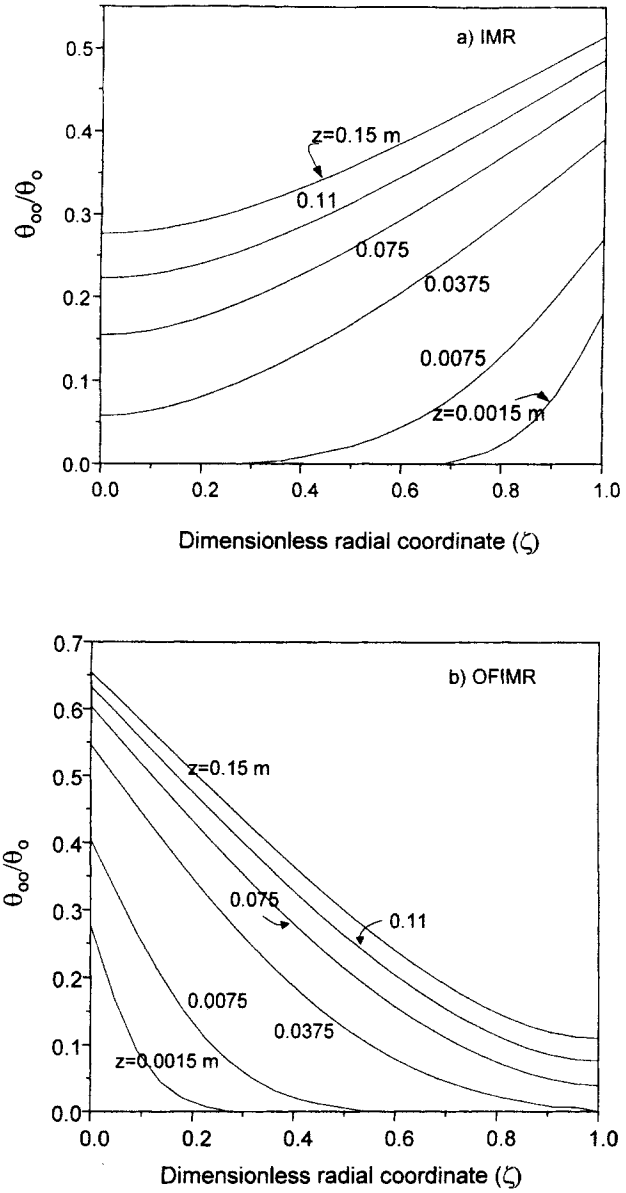

Figure 7. Evolution of concentration ratio of active selective and active nonselective sites (θ_{oo}/θ_o) along reactor radius for different axial positions: (a) IMR; (b) OFIMR.

Same conditions as in Figure 5.

As just shown, the most unfavorable conditions in the IMR (low θ_{oo}/θ_o ratio) occur at $\zeta \to 0$, near the reactor axis, where the temperature is also slightly higher compared to outer radial positions. The oxygen concentration profiles shown in Figure 5 indicate that at $z > 0.0375$ m (i.e., for most of the reactor length) a significant oxygen concentration exists in this region. Therefore the reaction will take place in the region of low ζ and its contribution to the total reaction will be largely nonselective. On the other hand, $\zeta \to 0$ is the favorable region (high θ_{oo}/θ_o ratio) in the OFIMR, and this is also the region where the highest reaction rate occurs, driven by the higher temperatures and oxygen concentrations. Due to the steep decrease of oxygen concentration shown in Figure 6, in the unfavorable zone ($\zeta \to 1$, low θ_{oo}/θ_o ratio) there is a very low oxygen concentration and the lowest temperature; in this way, the contribution of the unwanted reactions is minimized, which explains the higher selectivities obtained in the OFIMR.

Effect of operating conditions in the OFIMR

The performance of the OFIMR can be further increased by optimizing the operating conditions. Figure 9 shows the effect of temperature and of the overall O_2/butane ratio. At low values of the O_2/butane ratio the conversion of oxygen is high, and the increase in butane conversion with temperature is barely discernible (e.g., see the curve for O_2/butane = 0.67). Therefore increasing the temperature as a means of increasing the MA yield can only be contemplated for high enough O_2/butane ratios.

On the other, Figure 9 also shows that the selectivity increases with the O_2/butane ratio, while it decreases with temperature within the range studied. This decrease of selectivity is due to the negative effective of temperature in the reaction kinetics: the apparent activation energy is higher for the formation of CO and CO_2 than for the oxidation of bu-

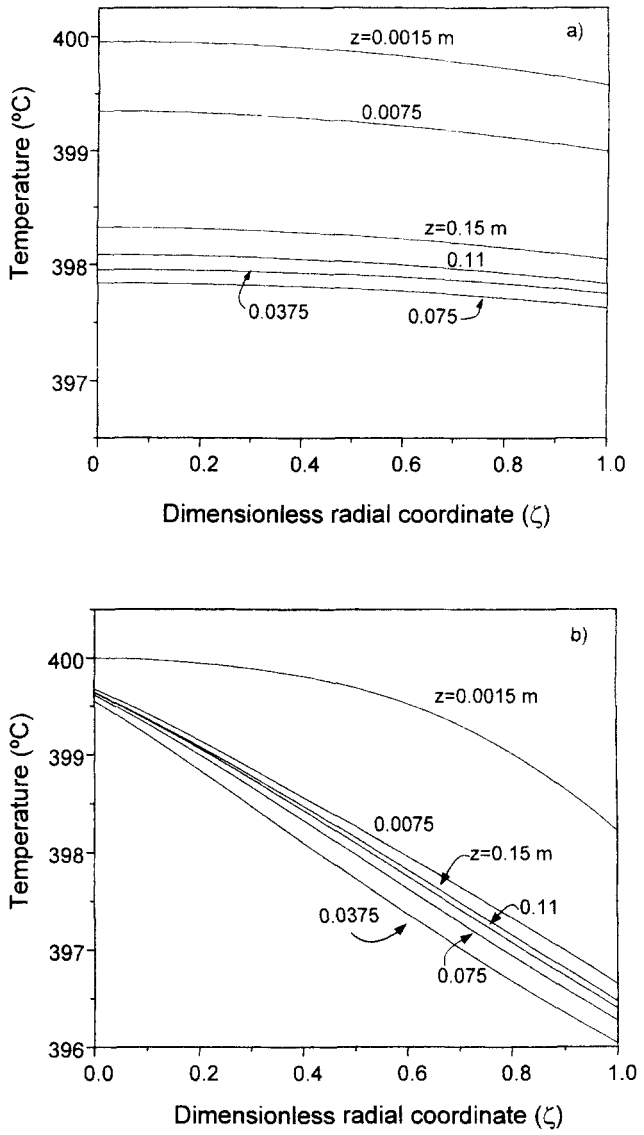

Figure 8. (a) Radial temperatures for the IMR and (b) OFIMR for different axial positions.

$\zeta = 0$ ($r = r_0$ in Figure 1), quartz thermowell in IMR and membrane wall in the OFIMR; $\zeta = 1$ ($r = r_1$ in Figure 1), membrane wall in IMR and outer reactor shell in OFIMR. Same conditions as in Figure 5.

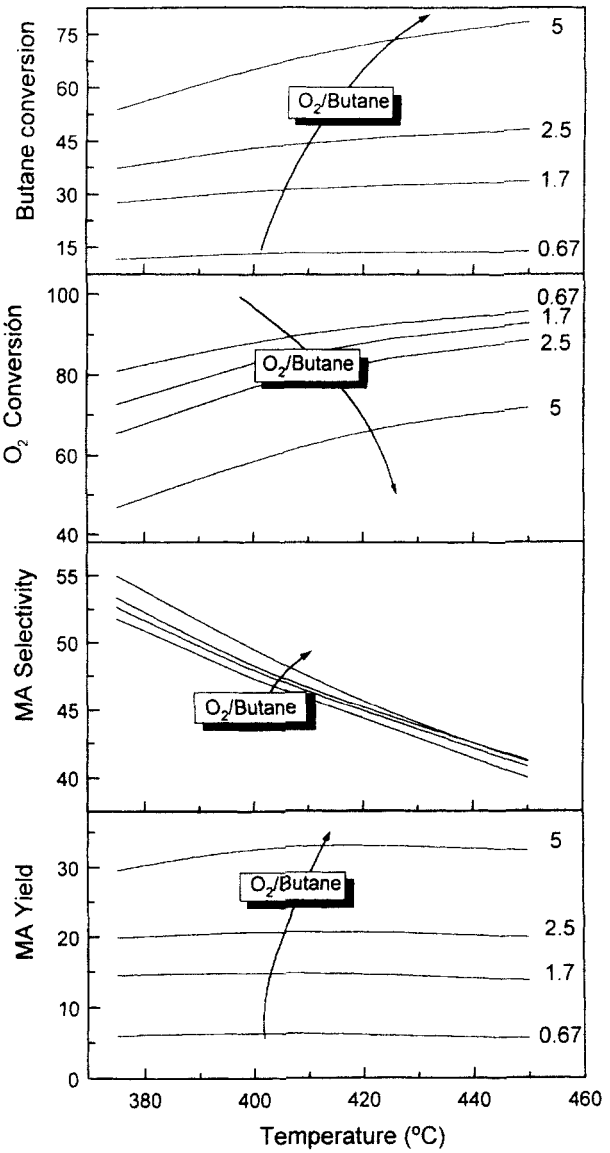

Figure 9. Butane and oxygen conversions, MA selectivity, and yield as a function of temperature and O_2/butane ratio, OFIMR.

Total feed flow: 8.3×10^{-6} m^3/s (STP). Oxygen concentration in the overall feed: 20%, variable butane concentration, rest He.

tane to MA (Mallada et al., 2000b), and this leads to a decrease in MA selectivity for higher temperatures. At low values of the O_2/butane ratio the decrease in selectivity overcomes the effect of temperature on butane conversion, and the yield decreases for increasing temperatures for most of the interval studied. At higher values of the O_2/butane ratio, the opposite is true, and thus the MA yield increases by about 3 percentage points as the temperature is raised from 375°C to 415°C. In general, the yield presents a shallow maximum at temperatures between 400 and 420°C, and the temperature corresponding to the maximum yield increases for higher values of the O_2/butane ratio.

Finally, Figure 10 shows the effect of the total flow rate for different values of the O_2/butane ratio at 400°C. While the butane and oxygen conversions follow the expected trend, decreasing with the flow rate, it is interesting to note that the MA selectivity increases markedly. This is due to the fact that at low flow rates, parts of the reactor are deprived of oxygen, and therefore the reaction takes place with a lower selectivity. As a consequence of the opposing trends shown by conversion and selectivity, a maximum exists in the MA yield with flow rate. The maximum is reached at higher flow rates as the O_2/butane ratio is depleted. At moderate values of the total flow rate and high values of the O_2/butane ratio, the model predicts MA yields in excess of 43%.

Conclusions

The radial concentration and temperature profiles need to be taken into account when explaining the results obtained

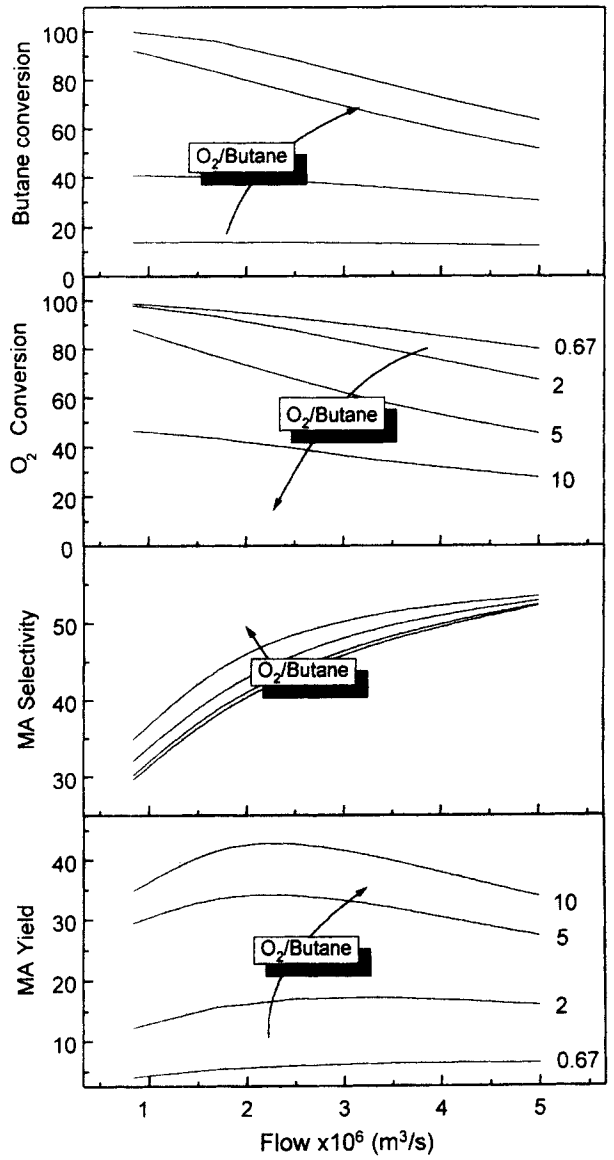

Figure 10. Butane and oxygen conversions, MA selectivity, and yield as a function of the total flow rate and O_2/butane ratio, OFIMR.

Oxygen concentration in the overall feed: 20%, variable butane concentration, rest He, T_o = 400°C.

not only with catalytic membrane reactors, but also in many instances of inert membrane reactors where the role of the membrane is solely the distribution of a reactant to a fixed bed of catalyst. The simulations carried out in this work show that, while there is only a moderate radial variation of temperature across the catalyst bed, large radial concentration gradients are possible. These are caused by the one-sided distribution of oxygen, coupled to a sufficiently fast rate of reaction.

In this work, the two different flow configurations studied (IMR and OFIMR) lead to a different radial variation of the oxygen and hydrocarbon concentrations, of temperature and of the concentration of active sites for the reaction. The considerably better performance that has been experimentally observed for the OFIMR can be explained by the fact that in this reactor the regions of higher reaction rate tend to coincide with the areas where the distribution of active sites is more favorable.

Acknowledgments

This work was carried out with financial support from the European Commission, Project BRPR-CT95-0046.

Notation

B_0 = permeability coefficient, m^2
C_{p_i} = specific heat of component i, kJ/(kmol·°C)
C = total molar concentration, kmol/m^3
D_{er} = effective radial diffusivity, m^2/s
D_{ik}^e = effective Knudsen diffusion coefficient, m^2/s
F_i = flow rate of component i, kmol/s or m^3/s
G = molar flux density, kmol/(m^2·s)
k_{er} = effective radial thermal conductivity, W/(m·K)
k_i = kinetic coefficient, Eqs. 1 to 3
K_0 = Knudsen coefficient, m
L = reactor length, m
M_i = molecular weight, kg/kmol
N_i = permeation flux, kmol/(m^2h)
P = reactor pressure, MPa
P_i = partial pressure of component i, MPa
$P_m = (P_{shell} + P_{tube})/2$, MPa
r_i = intrinsic reaction rate of component i, kmol/(kg_{cat}·s)
r_p = membrane pore radius, m
r = radial coordinate, m
r_1 = external radial coordinate (see Figure 1), m
r_0 = internal radial coordinate (see Figure 1), m
R = universal gas constant 8.314 kJ/(kmol·K)
T = temperature, °C
U = overall heat-transfer coefficient, W/(m^2·°C)
W = catalyst mass, kg
y_i = molar fraction of component i
z = axial coordinate, m

Greek letters

ΔH_j = heat of reaction j, kJ/kmol
ΔP = pressure drop across of membrane, MPa
δ = membrane thickness, m
μ = viscosity, N·s/m^2
θ_o = fraction of active nonselective sites
θ_{oo} = fraction of active selective sites
ρ_L = catalyst bed density, kg/m^3
$\zeta = (r - r_0)/(r_1 - r_0)$, dimensionless radial coordinate
$\phi = Z/L$, dimensionless axial coordinate

Subscripts

o = reactor inlet, $z = 0$
cm = cooling medium
B = n-butane

Abbreviations

DGM = dusty gas model
IMR = inert membrane reactor
MA = maleic anhydride
OFIMR = outward-flow inert membrane reactor
VPO = vanadium phosphate catalyst, often used in MA synthesis
W/F = space time

Literature Cited

Ait-Lachgar, K., A. Tuel, M. Brun, J. M. Herrmann, J. M. Krafft, J. R. Martin, J. C. Volta, and M. Abon, "Selective Oxidation of N-Butane to Maleic-Anhydride on Vanadyl Pyrophosphate—II—Characterization of the Oxygen-Treated Catalyst by

Electrical-Conductivity, Raman, XPS, and NMR Spectroscopic Techniques," *J. Catal.*, **177**, 224 (1998).
Bindjouli, A. B., Z. Dehouche, B. Bernauer, and J. Lieto, "Numerical Simulation of Catalytic Inert Membrane Reactor," *Comput. Chem. Eng.*, **18**, S337 (1994).
Centi, G., G. Fornasari, and F. Trifiró, "On the Mechanism of n-Butane Oxidation to Maleic Anhydride: Oxygen-Stoichiometry-Controlled Conditions," *J. Catal.*, **89**, 44 (1984).
Cheng, S., and X. Shuai, "Simulation of a Catalytic Membrane Reactor for Oxidative Coupling of Methane," *AIChE J.*, **41**, 1598 (1995).
Coronas, J., A. Gonzalo, D. Lafarga, and M. Menéndez, "Effect of the Membrane Activity on the Performance of an Inert Membrane Reactor," *AIChE J.*, **43**, 3095 (1997).
Coronas, J., and J. Santamaría, "Catalytic Reactors Based on Porous Ceramic Membranes," *Catal. Today*, **51**, 377 (1999a).
Coronas, J., and J. Santamaría, "Separations Using Zeolite Membranes," *Sep. Purif. Methods*, **28**, 127 (1999b).
De Wasch, A. P., and G. F. Froment, "Heat Transfer in Packed Beds," *Chem. Eng. Sci.*, **27**, 567 (1972).
Dixon, A. G., "Innovations in Catalytic Inorganic Membrane Reactors," *Catalysis*, **14**, 40 (1999).
Froment, G. F., and K. B. Hoffman, *Chemical Reactor Analysis and Design*, 2nd ed., Wiley, New York (1999).
Gear, C. W., *Numerical Initial Value Problems in Ordinary Differential Equations*, Prentice Hall, Englewood Cliffs, NJ (1971).
Harold, M. P., and C. Lee, "Intermediate Product Yield Enhancement with a Catalytic Inorganic Membrane: II. Nonisothermal and Integral Operation in Back-Mixed Reactor," *Chem. Eng. Sci.*, **52**, 1923 (1997).
Hutchings, G. J., A. Desmartinchomel, R. Olier, and J. C. Volta, "Role of the Product in the Transformation of a Catalyst to Its Active State," *Nature*, **368**(6466), 41 (1994).
Mallada, R., M. Pedernera, M. Menéndez, and J. Santamaría, "Synthesis of Maleic Anhydride in an Inert Membrane Reactor. Effect of Reactor Configuration," *Ind. Eng. Chem. Res.*, **36**, 620 (2000a).
Mallada, R., M. Pedernera, M. Menéndez, and J. Santamaría, manuscript in preparation (2000b).
Mason, E. A., and A. P. Malinauskas, "Gas Transport in Porous Media: The Dusty-Gas Model," *Chemical Engineering Monographs*, Elsevier, Amsterdam (1983).
Rodemerk, U., B. Kubias, H. W. Zanthoff, G. U. Wolf, and M. Baerns, "The Reaction Mechanism of the Selective Oxidation of Butane on $VO_2P_2O_7$ Catalysts: The Influence of the Valence State of Vanadium," *Appl. Catal. A: General*, **153**, 1997 217 (1997).
Saracco, G., J. W. Veldinsk, G. F. Versteeg, and W. P. M. van Swaaij, "Catalytic Combustion of Propane in a Membrane Reactor with Separate Feed of Reactants—I. Operation in Presence of Trans-Membrane Pressure Gradients," *Chem. Eng. Sci.*, **50**(17), 2833 (1995).
Saracco, G., H. W. J. P. Neomagus, G. F. Versteeg, and W. P. M. van Swaaij, "High-Temperature Membrane Reactors: Potential and Problems," *Chem. Eng. Sci.*, **54**, 1997 (1999).
Soejarto, A. D., G. W. Coulston, and G. L. Schrader, "In-Situ Laser Raman Spectroscopy During Sequential Oxidizing and Reducing Conditions for a Vanadium Phosphorus-Oxide," *Can. J. Chem. Eng.*, **74**, 594 (1996).
Sun, Y. M., and S. J. Khang, "A Catalytic Membrane Reactor: Its Performance in Comparison with Other Types of Reactors," *Ind. Eng. Chem. Res.*, **29**, 232 (1990).
Tavolaro, A., and E. Drioli, "Zeolite Membranes," *Adv. Mater.*, **11**, 975 (1999).
Téllez, C., M. Menéndez, and J. Santamaría, "Simulation of an Inert Membrane Reactor for the Oxidative Dehydrogenation of Butane," *Chem. Eng. Sci.*, **54**, 2917 (1999).
Tonkovick, A. L. Y., D. M. Jimenez, J. L. Zilka, and G. L. Roberts, "Inorganic Membrane Reactors for the Oxidative Coupling of Methane," *Chem. Eng. Sci.*, **51**, 3051 (1996).
Tsai, C. Y., Y. H. Ma, W. R. Moser, and A. G. Dixon, "Modeling of a Nonisothermal Catalytic Membrane Reactor," *Chem. Eng. Commun.*, **134**, 107 (1995).
Tsotsis, T. T., A. M. Champagne, S. P. Vasileiadis, Z. D. Ziaka, and R. G. Minet, "Packed Bed Catalytic Membrane Reactors," *Chem. Eng. Sci.*, **47**, 2903 (1992).
Yang, C., N. Xu, and J. Shi, "Experimental and Modeling Study on a Packed-Bed Membrane Reactor for Partial Oxidation of Methane to Formaldehyde," *Ind. Eng. Chem. Res.*, **37**, 2601 (1998).

Manuscript received Jan. 31, 2000, and revision received May 15, 2000.